Original Research Article

Interactions of Kratom Alkaloids–Mitragynine, 7-Hydroxymitragynine, and Mitragynine Pseudoindoxyl with Lipid Bilayers: A Molecular Dynamics Study

Nur Syahirunelisa Mohd Zubri[1], Nur Alya Amirah Azhar[1], Nur Aqasyah Amran[1], Shirley Weng In Siu[2], Asmah Awal[3] and Siti Azma Jusoh[1]*

[1]Faculty of Pharmacy, Universiti Teknologi MARA Kampus Puncak Alam, 42300 Bandar Puncak Alam, Selangor, Malaysia.
[2]Centre for Artificial Intelligence Driven Drug Discovery, Faculty of Applied Sciences, Macao Polytechnic University, R. de Luís Gonzaga Gomes, Macau SAR 999078, China.
[3]Faculty of Plantation and Agrotechnology, Universiti Teknologi MARA Cawangan Melaka, Kampus Jasin, 77300 Merlimau, Melaka, Malaysia.

ABSTRACT

Kratom, a plant native to Southeast Asia, has gained attention as a potential alternative to opioids for pain relief and managing withdrawal symptoms. However, concerns about its safety persist due to reported adverse effects and drug interactions. Despite having at least 50 alkaloids, the pharmacological properties of kratom remain poorly understood due to limited research. In this study, molecular dynamics (MD) simulations were employed to investigate interactions of three major alkaloids of kratom—mitragynine, 7-hydroxymitragynine, and mitragynine pseudoindoxyl—with a dipalmitoylphosphatidylcholine (DPPC) lipid bilayer. These alkaloids were initially placed in the aqueous phase in order to allow for unbiased diffusion into the lipid bilayer. The simulation revealed rapid permeation of all three compounds, with mitragynine exhibiting the fastest insertion time (~16 ns), followed by mitragynine pseudoindoxyl (~32 ns) and 7-hydroxymitragynine (~33 ns). Upon entry, they predominantly localized near the lipid-water interface, forming hydrogen bonds with both water molecules and lipid phosphate groups. Mass density profiles and distance analyses further demonstrated that mitragynine and mitragynine pseudoindoxyl remained closer to the lipid headgroups, while 7-hydroxymitragynine penetrated deeper into the hydrophobic core. These findings highlight the amphiphilic nature of kratom alkaloids, with a tendency for hydrophobic interactions, consistent with their physicochemical properties. In conclusion, this is the first study that provides fundamental insights into the membrane partitioning behavior of kratom alkaloids, emphasizing their rapid permeation and bilayer localization. Such knowledge could guide the rational design of safer and more effective therapeutics for pain management, opioid withdrawal, and other pharmacological applications, addressing the need for alternatives to classical opioids.

Keywords: kratom; alkaloids; molecular dynamics simulations; DPPC; lipid bilayer, mitragynine, 7-hydroxy-mitragynine, mitragynine pseudoindoxyl

Corresponding author
Siti Azma Jusoh
Department of Pharmacology and Life Sciences, Faculty of Pharmacy, Universiti Teknologi MARA, Kampus Puncak Alam, 42300 Bandar Puncak Alam, Selangor, Malaysia.
Email: sitiazma@uitm.edu.my

Received: 14 Jan 2025; accepted: 08 May 2025
Available online: 30 May 2025 http://doi.org/10.24191/IJPNaCS.v8i1.09

Copyright© 2025 UiTM Press. This is an open access article licensed under CC BY-SA
https://creativecommons.org/licenses/by-sa/4.0/

1.0 Introduction

Mitragyna speciosa, commonly known as kratom (or "ketum" in Malaysia), is a psychoactive plant native to Thailand, Malaysia, and Indonesia, where it has been traditionally consumed by chewing or brewing its leaves to relieve fatigue and pain. The plant's legal status varies widely across the region: Malaysia prohibits it under the Poisons Act 1952 (1), penalizing possession despite allowing cultivation; Singapore enforces a strict ban with severe penalties; Thailand legalized kratom in 2021, removing it from the narcotics list to regulated medical and traditional use (2); while Indonesia permits commercial export but restricts domestic consumption through unwritten policies, despite lacking official legislation. In Western countries, kratom has gained popularity primarily for self-treatment rather than recreation. According to the survey in the US in 2021, more than 60% kratom users using it as alternative therapy for chronic pain management, 20-30% for anxiety and depression symptoms, and ~15% for opioids withdrawals (3, 4). Despite warnings from the U.S. Food and Drug Administration (FDA) about potential risks, kratom remains federally unregulated in the U.S (5).

Reports show kratom can cause nausea, dizziness, and constipation, while heavy use risks liver damage, seizures, and heart issues. Dependence and withdrawal are well documented. More dangerously, adulterated products often contain synthetic opioids or heavy metals, linked to fatal overdoses. The FDA warns against use, especially with other substances, due to these unpredictable risks (5-8).

The pharmacological properties of kratom stem from its diverse alkaloid profile, with more than 50 natural alkaloids identified (9, 10). Among these, mitragynine and 7-hydroxymitragynine are the most extensively studied (11). Mitragynine constitutes approximately 66% of the crude alkaloid content, while 7-hydroxymitragynine accounts for less than 1% (12). Both alkaloids exhibit opioid-like effects, acting as partial agonists of the μ-opioid receptor (MOR) and weak agonists of the κ-opioid (KOR) and δ-opioid (DOR) receptors (11,13). These receptors belong to the G-protein-coupled receptor (GPCR) superfamily, which features a conserved structure comprising seven transmembrane α-helices interspersed with extracellular and intracellular loops (14). While MOR activation underpins the analgesic effects of opioids, it is also associated with undesirable side effects such as dependence, tolerance, respiratory depression, and gastrointestinal disturbances (15,16). Interestingly, mitragynine and 7-hydroxymitragynine have garnered significant attention as potential alternatives to classical opioids for pain management and other therapeutic applications. Several studies reported that mitragynine exhibited analgesic effects through partial agonism at MOR, while displaying a lower risk of respiratory depression compared to traditional opioids such as morphine (12, 17, 18). Similarly, 7-hydroxymitragynine, a potent metabolite of mitragynine, has demonstrated enhanced analgesic activity, making it a promising candidate for pain relief (12, 17, 19). Mitragynine pseudoindoxyl, another derivative, has shown potential as a biased agonist to opioid receptors, offering a pathway to develop safer and more effective analgesics (20). These three alkaloids are shown to be more potent than morphine, while exhibit less addiction effects, thus making them attractive compounds for therapeutics usage.

Studies using animal models, receptor-binding assays, and computational approaches further revealed that mitragynine and 7-hydroxymitragynine possessed high affinities for opioid receptors, and mitragynine pseudoindoxyl demonstrated strong interactions with both MOR and DOR but moderate affinity for KOR (8, 17). Comparatively, synthetic opioids such as fentanyl exhibit markedly higher potency at

MOR, being over 50 times more potent than morphine (21, 22). Notably, fentanyl rapidly partitioned into lipid bilayers and directly interacted with the MOR orthosteric pocket via membrane penetration, meanwhile morphine swiftly migrated from water milieu to lipid environment (23, 24). These findings highlight the critical role of membrane dynamics in facilitating ligand-receptor interactions and underscore the potency of fentanyl relative to both mitragynine and morphine (19, 25).

Interactions between drugs or natural products and cellular membranes are essential for understanding their pharmacokinetics and pharmacodynamics. Physicochemical properties such as lipophilicity, charge, and size influence a compound's ability to traverse phospholipid bilayers, ultimately determining receptor accessibility (26, 27). For example, opioids such as fentanyl and morphine utilize distinct membrane-mediated pathways to reach their target receptors (23, 24). Similarly, cannabinoids have been shown to directly access receptor binding pockets via lipid membranes (28). Despite the significant pharmacological interest in kratom alkaloids, their interactions with membrane lipids remain poorly characterized due to limited studies.

MD simulations have become an indispensable tool for studying drug-membrane interactions, offering atomic-level insights into the behavior of drug molecules within lipid bilayers (29-31). Unlike experimental techniques, MD simulations allow researchers to observe dynamic processes such as drug penetration, localization, and aggregation in real-time (32). This is particularly valuable for understanding the behavior of amphiphilic drugs that exhibit complex interactions with lipid bilayers due to their dual affinity for polar and nonpolar environments (33). Using MD simulations, predictions can be made for drug bioavailability, membrane permeability, and potential pharmacological effects, providing a foundation for rational drug design and optimization (32). Therefore, in this study, we employed all-atom MD simulations to investigate the interactions of kratom alkaloids; mitragynine, 7-hydroxymitragynine, and mitragynine pseudoindoxyl—with lipid bilayers. Our findings provide detailed atomic-level insights into the dynamics and energetics of these interactions, contributing to a deeper understanding of kratom's pharmacology and its potential as a therapeutic agent.

2.0 Materials and Methods

2.1 Ligand Preparation

All selected ligands were chosen because previous research demonstrated their agonistic binding to the μ-opioid receptor (8). Structural information of the three kratom alkaloids: mitragynine, 7-hydroxymitragynine and mitragynine pseudoindoxyl were obtained from the PubChem database (https://pubchem.ncbi.nlm.nih.gov/), PubChem ID: 3034396, 44301524, 44301701, respectively. The Automated Topology Builder (ATB) (https://atb.uq.edu.au/) server (34) was utilized to obtain GROMACS topology files for the alkaloid molecules to be used for the MD simulations. In ATB, the net charge of each alkaloid was set to 0 for the neutral state, while for the protonated state, it was set to +1.

2.2 Alkaloid-Lipid System Setup

The input structures of the pre-equilibrated lipid bilayer of 128 dipalmitoyl-phosphatidylcholine (DPPC) lipids were obtained from our previous study (35). The simulation box for the lipid bilayer-water system was set to 6.418 × 6.443 × 8.000 nm. In each system, an alkaloid compound was positioned in the water environment approximately more than 10 Å distance from the nearest lipid headgroup and the box edges. The systems were solvated with a total of 6169 water molecules. Counterions Na+ and Cl- were added to neutralize the overall charge of the system.

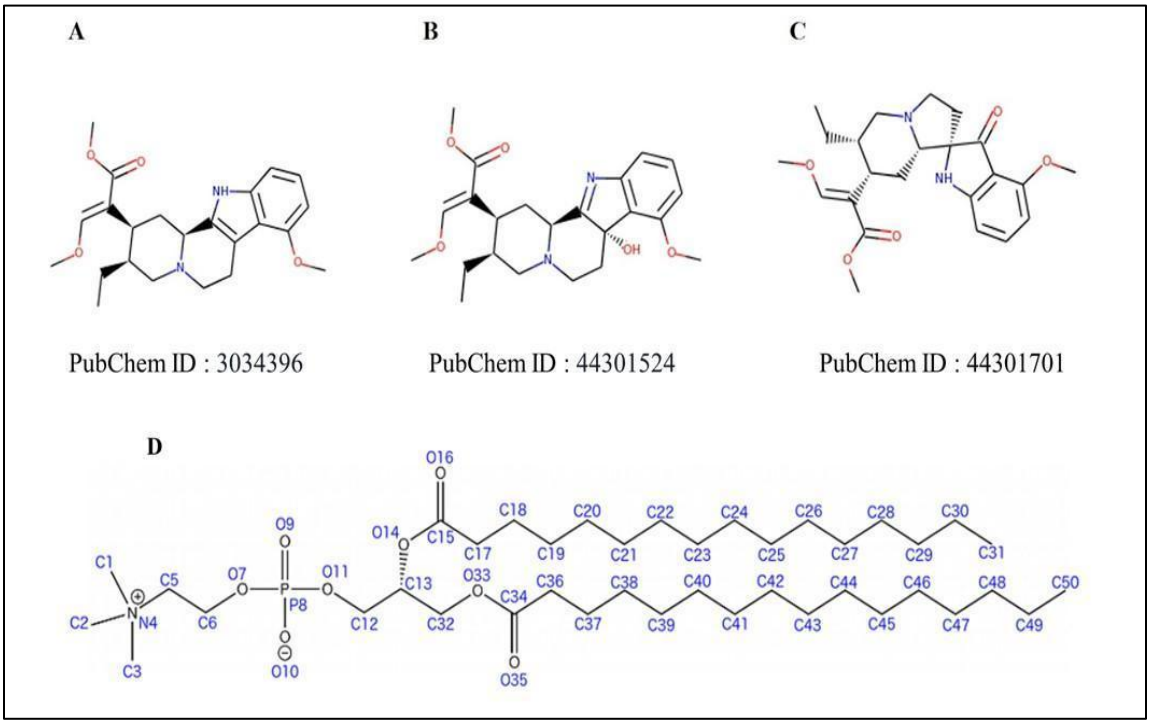


Figure 1: 2D structures of **(A)** mitragynine, **(B)** 7-hydroxymitragynine, **(C)** mitragynine pseudoindoxyl and **(D)** DPPC.

2.3 Molecular Dynamics Simulations

MD simulations were performed using the GROMACS software package 2021.5 (34, 36, 37) using GROMOS-54A7 force field (36, 38) with a modified version of parameter 54A7 to include Berger lipid parameters of the DPPC lipids. The SPC (Simple Point Charge) model was used to represent the water (39). Prior to the production simulations, the initial systems were subjected to 1000 steps of energy minimization using the steepest descent algorithm to remove interatomic clashes, followed by the canonical NVT (constant temperature), and NPT (constant pressure) equilibrations. The long-range Coulombic interactions were evaluated using Particle Mesh Ewald (PME) method (40) with a cutoff set at 1.2 nm. For the van der Waals interactions, a cutoff distance of 1.2 nm was used. Bonds to H atoms were constrained using the LINCS algorithm (41). Periodic boundary conditions were used in all directions. The temperature for the DPPC was stabilized at 323 K with a time constant of τT= 0.1 ps. All production simulations were carried out for 100 ns each with a timestep of 2 fs under the isothermal-isobaric (NPT) ensemble, which maintains a constant number of particles, temperature and pressure. Production run for each set of systems was repeated three times (triplicates) to obtain statistics.

Partial density of the system, root mean square deviation (RMSD), distance of the alkaloids to the membrane and hydrogen bond analyses were computed using the GROMACS internal tools. The output data were analyzed using the XMGrace program (https://plasma-gate.weizmann.ac.il/Grace/), and the plots were prepared using Gnuplot (http://www.gnuplot.info/) (42). The PyMOL program (43, 44) was used for visualization,

interaction analysis and for making images. The area per lipid and the thickness of the bilayer were analyzed by using the GridMAT-MD scripts (45).

3.0 Results

3.1 Overall Observation During the Alkaloid-Lipid Bilayer Simulations

MD simulation is a powerful tool for studying the membrane permeability of small molecules. Explicit all-atom MD simulations provide detailed insights into atomic interactions within a system that mimics the natural environment of the target molecule. While experimental methods offer valuable information about membrane interactions, they often lack the temporal and spatial resolution to capture dynamic processes, such as the real-time permeation of molecules through lipid bilayers or the formation of transient interactions at the atomic level. MD simulations address these limitations by providing a high-resolution, time-resolved view of molecular behavior, making them an essential complement to experimental studies.

In this study, we employed MD simulations to investigate the behavior of kratom alkaloids in membrane lipid bilayers. To model the cell membrane, we used a DPPC lipid bilayer, a widely accepted and computationally efficient representation of mammalian cell membranes. While real cell membranes are composed of diverse lipid species, DPPC serves as a well-characterized model system that captures the essential physicochemical properties of lipid bilayers, such as phase behavior, fluidity, and permeability. Its simplicity allows for clear interpretation of molecular interactions, making it an ideal starting point for understanding the membrane partitioning behavior of kratom alkaloids. The use of DPPC as a model membrane is well-supported in the literature. For instance, high-impact studies have extensively utilized DPPC bilayers to investigate the interactions of small molecules, peptides, and drugs with lipid membranes (46–48). These studies demonstrate that DPPC provides a reliable and reproducible platform for elucidating fundamental membrane processes, such as permeation, partitioning, and molecular orientation at the lipid-water interface. By adopting this established approach, our work aligns with prior research while contributing new insights into the behavior of kratom alkaloids.

Based on the simulation trajectories, the behavior of the alkaloids was visualized throughout the 100 ns MD simulations. Overall, all three kratom alkaloids—mitragynine, 7-hydroxymitragynine, and mitragynine pseudoindoxyl—rapidly penetrated the lipid bilayer within 40 ns (Figure 2). Among the alkaloids, mitragynine demonstrated the fastest translocation from the bulk aqueous environment, occurring in approximately 16 ns, likely due to its structure that facilitating quicker interactions with the hydrophobic core. The relatively small and planar structure of mitragynine may contribute to its efficient bilayer penetration and stable interaction within the membrane (Figure 2A). Mitragynine pseudoindoxyl and 7-hydroxymitragynine followed with nearly identical penetration times of 32 ns and 33 ns, respectively. Their slightly slower penetration compared to mitragynine may be due to the presence of the pseudoindoxyl and hydroxyl groups, which could form additional interactions with the lipid headgroups. Upon entry, all three alkaloids remained localized beneath the lipid headgroup region for the remainder of the 100 ns simulation, stabilizing in this position and indicating strong hydrophobic interactions with the membrane. This consistent bilayer penetration behavior highlights the potential of the kratom alkaloids for efficient membrane integration, which could influence

their pharmacokinetics and interactions with cellular membranes.

3.2 Dynamics Analyses of the Alkaloid-Lipid Bilayer Model Systems

Key properties of lipid bilayers, such as area per lipid and membrane thickness are essential for assessing their structural integrity and behavior. Among these, the area per lipid is a critical parameter, as it provides insights into the structural organization of the lipid bilayer, and validates the accuracy of the simulation models and force fields. In this study, the area per DPPC molecule was determined by tracking the positions of all atoms over time and calculating the average area occupied by each lipid. This was achieved by summing the areas of all lipid molecules and dividing by the total number of lipids, yielding the mean area per lipid.

For the pure DPPC bilayer, the area per lipid was measured as 0.646 ± 0.02 nm², consistent with established values. Upon the introduction of neutral alkaloids, the area per lipid increased to 0.753 ± 0.04 nm², indicating that the alkaloids disrupted lipid packing and expanded the surface area. In contrast, the presence of the protonated alkaloids resulted in an area per lipid of 0.698 ± 0.03 nm², reflecting a smaller expansion compared to neutral alkaloids but still larger than the pure DPPC system (Table 1). These observations suggest that neutral alkaloids exert a more pronounced effect on lipid packing than protonated alkaloids.

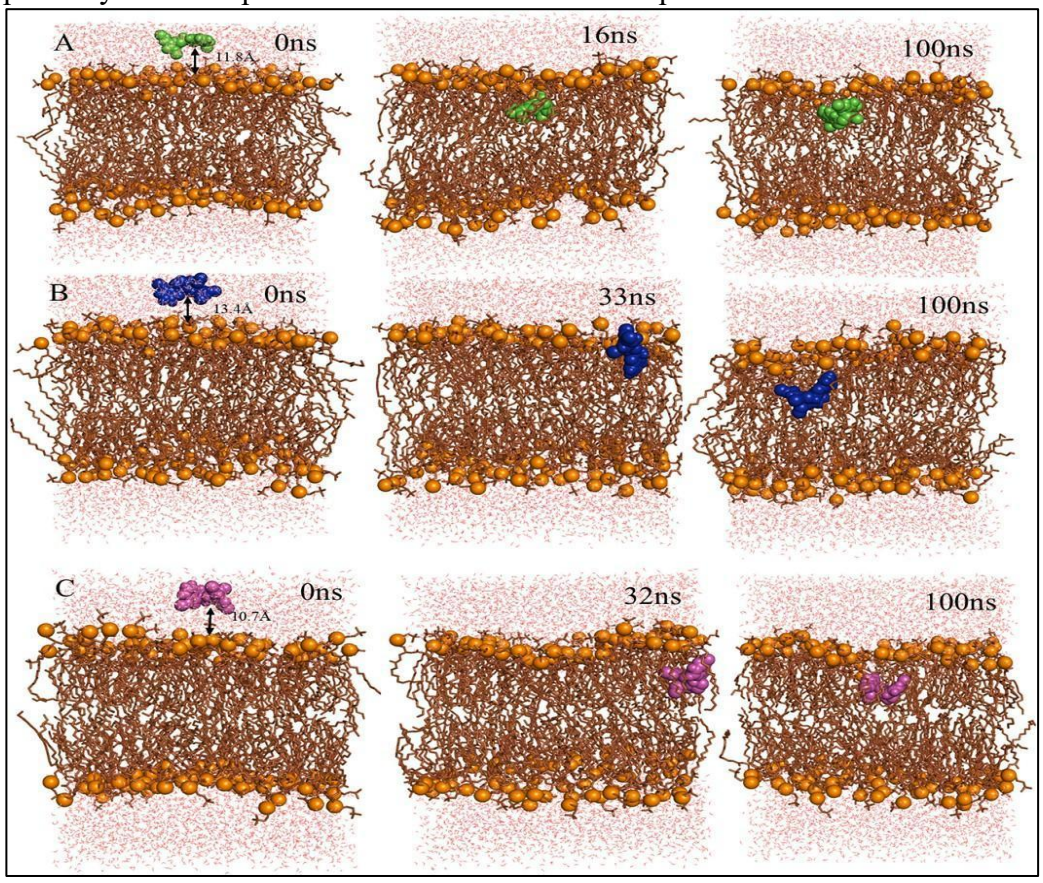


Figure 2: Interactions of kratom alkaloids with DPPC lipid bilayers during the 100 ns MD simulations. Snapshots of the final simulation trajectory for the alkaloid-DPPC systems: **(A)** mitragynine (green spheres), **(B)** 7-hydroxymitragynine (blue spheres), and **(C)** mitragynine pseudoindoxyl (magenta spheres). Other molecules in the systems are lipid headgroup (orange spheres), lipid tails (brown sticks) and water (red sticks).

Table 1: Analyses of area per lipid and membrane thickness for the pure DPPC lipid bilayer and the alkaloid-DPPC bilayer systems during the 100 ns of MD simulations.

Bilayer property	DPPC only	DPPC-Neutral Alkaloid	DPPC-Protonated Alkaloid	Experimental References	References (MD simulation DPPC only)
Area per Lipid (nm^2)	0.646 ± 0.02	0.753 ± 0.04	0.698 ± 0.03	0.633-0.729 (49)	0.600 (39) 0.655 (50)
Membrane Thickness (nm)	3.895 ± 0.01	3.912 ± 0.01	3.943 ± 0.02	3.83 (49)	3.60 (39)

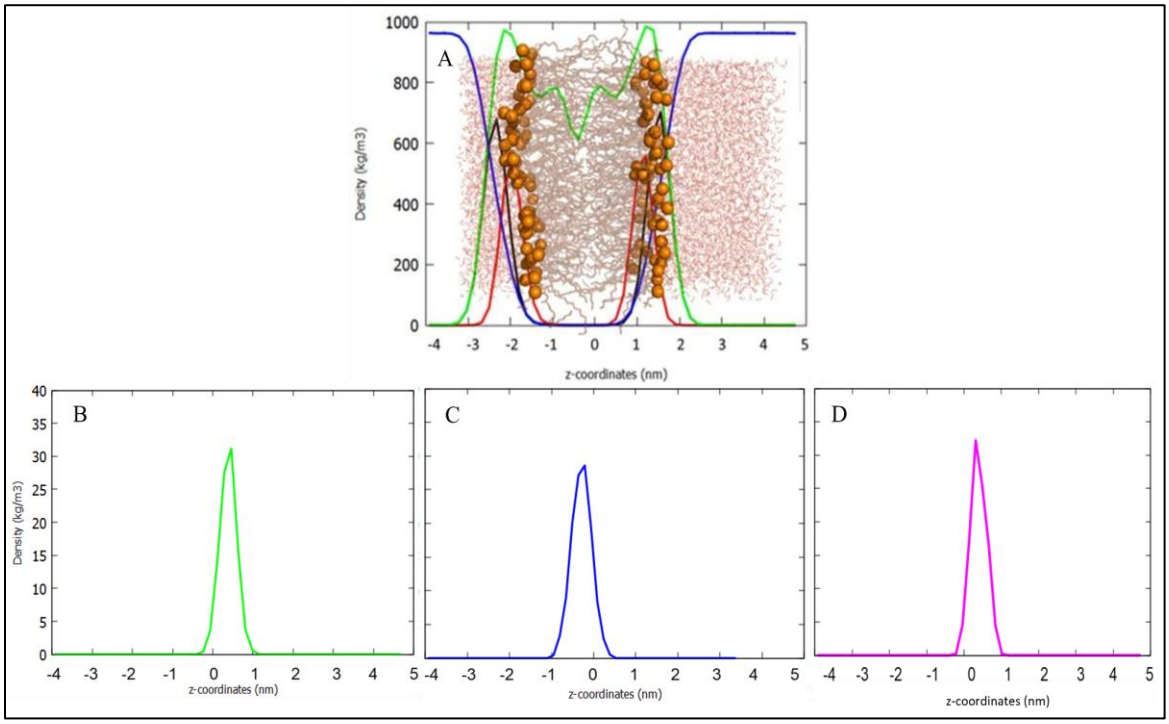


Figure 3: The mass densities of a single kratom alkaloid in DPCC lipid bilayer during the 100 ns MD simulation. **(A)** The snapshot of 100 ns DPPC bilayer overlayed with the mass density profile of the pure lipid bilayer system. Headgroups (black), glycerol ester (red), acyl chains (green), water (blue), lipid headgroup (orange spheres), lipid tails (brown sticks) and water (red sticks). The mass densities plots of kratom alkaloids in DPPC lipid bilayer: **(B)** mitragynine (green line), **(C)** 7-hydroxymitragynine (blue line) and **(D)** mitragynine pseudoindoxyl (magenta line).

Notably, all measured values remained within the physiological range for DPPC lipids (0.629 - 0.712 nm^2), as reported in experimental studies (39, 49, 50). Similarly, membrane thickness was evaluated for all systems (Table 1). For the pure DPPC bilayer, the membrane thickness was 3.895 ± 0.01 nm, in close agreement with experimental data (49) and previous MD simulations (39).

In the presence of neutral and protonated alkaloids, the membrane thickness increased slightly to 3.912 ± 0.01 nm and 3.943 ± 0.02 nm, respectively. This increase suggests that the insertion of alkaloid molecules enhances the ordering of lipid acyl chains, resulting in a thicker membrane structure. Importantly, the membrane thickness values for all systems remained within the physiological range for DPPC lipids (49).

The mass density profile is another fundamental property used to characterize the structural organization of lipid bilayers at the molecular level. It provides a spatial distribution of the mass density of different components (e.g., lipid headgroups, tails, water, and embedded molecules) along the axis perpendicular to the bilayer plane (z-axis). This profile is essential for understanding the arrangement and dynamics of lipids and other molecules within the membrane, as well as their interactions with the surrounding environment. In this study, the mass density profiles of all model systems were computed during the final 50 ns of the simulations. This is to ensure that the systems already converged and reach stable configuration. In all simulations of alkaloid-DPPC systems, the mass density distribution of the major molecules within the lipid bilayer closely matches the mass densities of the pure DPPC lipid-water system (Figure 3 (A)). This indicates the overall structure and organization of the DPPC lipid bilayer remains stable during the presence of a kratom alkaloid.

Based on the individual analysis of each alkaloid, the density distribution exhibited their positions averagely located at the acyl chains of the DPPC lipid bilayer, which indicate their preference to interact with hydrophobic molecules. As shown from Figure 3, mitragynine and mitragynine pseudoindoxyl molecules exhibit similar density distributions (z position between 1 to 0), with the peak at 0.48 ± 0.14 nm and 0.33 ± 0.18 nm, respectively. Meanwhile, the 7-hydroxymitragynine molecule shows its density peak at -0.72 ± 0.15 nm, which indicates that its locations average at the other lipid leaflet. The density analysis indicates that these alkaloids are able to penetrate deeper into the hydrophobic core region, nevertheless still interacting with the polar region of the lipid bilayers as illustrated in Figure 2.

3.2 Inter-molecular Interactions of Kratom Alkaloids with DPPC Lipid Bilayer and Water Molecules

Interactions between the kratom alkaloids and lipid bilayer was evaluated based on the distance between the alkaloid molecules to the phosphate head groups of the lipid bilayer throughout the 100 ns MD simulations. Figure 4 shows the average distance of each alkaloid from their initial position in the water phase to the time when they start to penetrate the lipid bilayer, and then when they subsequently localize beneath the lipid headgroups till the end of the simulations.

During the simulations, all the three alkaloids were observed to enter the lipid bilayer within 40 ns in the initial run. The interaction between the alkaloid molecules and the bilayer was detected at a distance of approximately 3 nm. Among the three alkaloids, mitragynine exhibited the fastest interaction with the lipid bilayer in the first run, penetrating within ~16 ns.

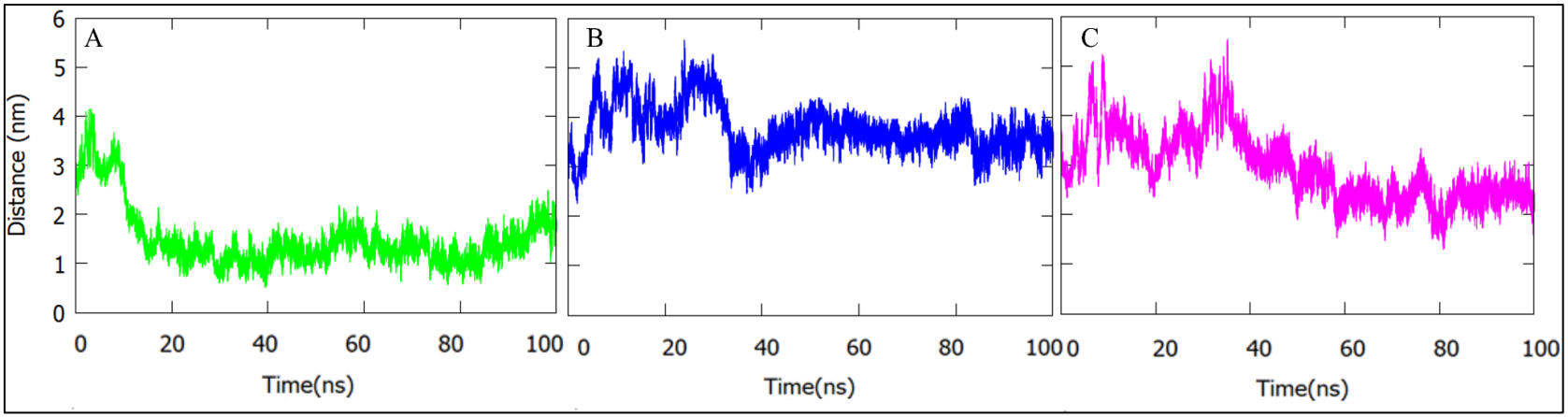


Figure 4: Distances between the alkaloids and the lipid headgroups during the 100 ns MD simulations. MD simulations of **(A)** mitragynine (green), **(B)** 7-hydroxymitragynine (blue), and **(C)** mitragynine pseudoindoxyl (magenta).

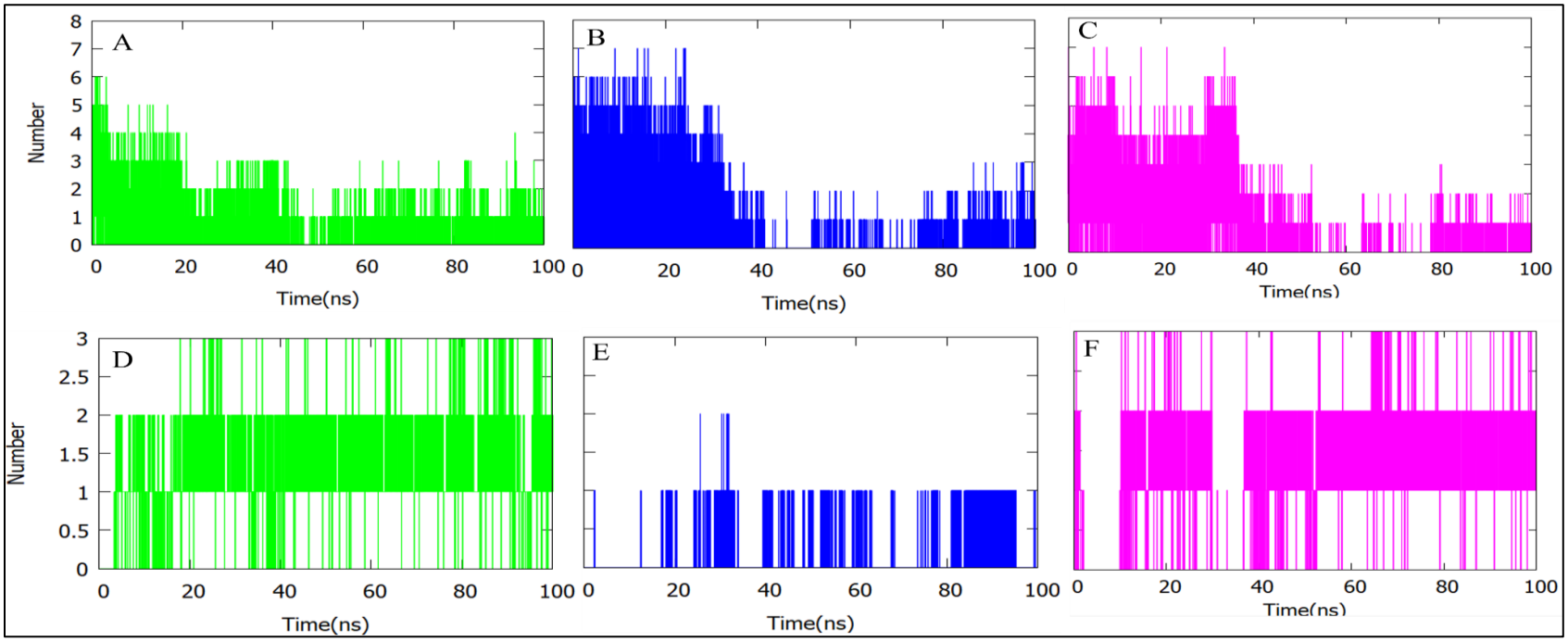


Figure 5: Hydrogen bond interactions between the alkaloids and water molecules **(A, B, C),** and lipid **(D, E, F)** during the 100 ns MD simulations. MD simulations of mitragynine **(A, D)**, 7-hydroxymitragynine **(B, E)**, and mitragynine pseudoindoxyl **(C, F)**.

Over the final 50 ns of the simulations, mitragynine remained closest to the polar head groups of the lipids, as evidenced by an average distance of 1.23 ± 0.71 nm between mitragynine and the lipid head groups. In contrast, 7-hydroxymitragynine and mitragynine pseudoindoxyl penetrated the bilayer more slowly in the initial run, taking approximately ~30 ns to interact with the lipid bilayer. By the end of the simulations, both alkaloids positioned themselves further from the lipid head groups compared to mitragynine. The average distances for mitragynine pseudoindoxyl and 7-hydroxymitragynine were 2.40 ± 0.31 nm and 3.62 ± 0.27 nm, respectively. These results suggest that 7-hydroxymitragynine and mitragynine pseudoindoxyl preferentially localize in more hydrophobic regions of the bilayer, reflecting their stronger affinity for hydrophobic environments compared to mitragynine. However, it is important to note that these results represent the first run of the simulation. In one of the three replicate runs, mitragynine exhibited insertion only after 50 ns (Supplementary Figure 1), suggesting that the type of alkaloid may not be the sole determinant of penetration speed. Variability in insertion times across replicates highlights the influence of random or unpredictable factors, such as the initial orientation of the molecules or random movements caused by thermal energy during the permeation process.

Hydrogen bond analysis was performed to provide detailed insights into the interactions between the alkaloids and the lipid bilayer (Figure 5). In this study, hydrogen bond interactions were calculated for both water molecules and DPPC lipids. For interactions with water, hydrogen bonds were identified between the oxygen atoms of water and the hydrogen atoms of polar functional groups in the alkaloids, such as hydroxyl or amine groups. These interactions reflect the ability of the alkaloids to form stable hydrogen bonds with the aqueous environment. For interactions with DPPC lipids, hydrogen bonds were analyzed between the polar headgroups of the lipids and the alkaloids. Specifically, the phosphate oxygen atoms and ester carbonyl oxygen atoms of the DPPC lipid headgroups served as hydrogen bond acceptors, while the hydrogen atoms of the alkaloids' polar functional groups acted as hydrogen bond donors.

During the simulations, given that the alkaloids were initially positioned in the water phase, they formed a significant number of hydrogen bonds with water molecules at the beginning. As shown in Figure 5 (A, B, and C), the three alkaloids were able to form up to seven hydrogen bonds with water molecules before entering the lipid bilayer. However, as the simulation progressed, the alkaloids diffused toward the lipid bilayer, resulting in a gradual reduction in hydrogen bonds with water as they began to interact more with the lipid headgroups. Then, after localizing within the bilayer, the number of hydrogen bonds with water decreased to an average of two for mitragynine and one for 7-hydroxymitragynine and mitragynine pseudoindoxyl. Nevertheless, even after residing in the lipid region, the alkaloids remain interacting with water molecules. This is attributed to their predominant localization near the lipid-water interface, where they positioned themselves beneath the lipid headgroups but remained accessible to the aqueous phase. Furthermore, the polar headgroups of the DPPC lipids are hydrated and interact with water molecules at the interface. Consequently, the amphiphilic nature of the alkaloids allows them to form hydrogen bonds with water molecules drawn into the lipid interface.

In contrast to the hydrogen bond interactions with water, interactions with the lipid headgroups were minimal at the start of the simulations. This was logical, as the alkaloids were initially located in the water

phase, far from the lipid bilayer. However, as the simulation progressed and the alkaloids began to interact with the lipid bilayer, hydrogen bond formation with the lipid headgroups increased. The increase in hydrogen bonds with the lipid headgroups coincided with the penetration of the alkaloids into the bilayer. Specifically, the polar functional groups of the alkaloids, such as hydroxyl and amine groups, formed hydrogen bonds with the phosphate oxygen atoms and ester carbonyl oxygen atoms of the DPPC lipid headgroups. Based on the observations during the simulations (Figure 5 (D, E and F)), mitragynine and mitragynine pseudoindoxyl formed hydrogen bonds with the DPPC lipids before fully entering the lipid region. After localizing within the bilayer, both alkaloids continued to form at least two strong hydrogen bonds with the lipid headgroups until the end of the simulations, indicating their preference to remain close to the lipid headgroups. In contrast, 7-hydroxymitragynine began forming hydrogen bonds with the lipid bilayer at approximately 20 ns, consistent with its later insertion into the bilayer at ~30 ns. After residing in the lipid bilayer, 7-hydroxymitragynine maintained an average of one hydrogen bond interaction with the lipid headgroups. From the plots, there were periods where absent hydrogen bonds were observed, which illustrated that 7-hydroxymitragynine occasionally localized deeper into the hydrophobic core region. This behavior aligns with the mass density profile of 7-hydroxymitragynine (Figure 3C), which shows its average density positioned deeper to the other lipid leaflet, farther from the polar headgroup region. At this depth, 7-hydroxymitragynine is less accessible to the lipid headgroups, explaining the absence of hydrogen bonds during these intervals.

The hydrogen bond analysis revealed opposite trends for interactions with water and lipid headgroups during the simulation. The alkaloids formed numerous hydrogen bonds with water during the initial stage but showed minimal interactions with lipids. As they penetrated the bilayer, hydrogen bonds with water decreased, while those with lipid headgroups increased, reflecting their transition from the aqueous phase to the lipid environment. This behavior aligns with the positions of the alkaloids in the lipid bilayer system.

4.0 Discussion

In this study, findings from MD simulations revealed distinct yet consistent behaviors among the kratom alkaloids, highlighting their interactions with DPPC lipid bilayers. Mitragynine, 7-hydroxymitragynine, and mitragynine pseudoindoxyl exhibited amphiphilic behavior, localizing near the lipid headgroups while embedding in the hydrophobic core. These amphiphilic molecules formed hydrogen bonds with the polar headgroups of DPPC lipids as well as with the water molecules at the lipid-water interface. This dual behavior is consistent with known amphiphilic drugs, such as fentanyl and buprenorphine, which also exhibit membrane localization near lipid headgroups (12, 17). Fentanyl was reported to orient itself parallel to the headgroups while forming interactions with the water molecules at the interface that lead to disruption of lipid ordering, while propofol, a general anesthetic, prefers to interact with the carbonyl oxygen groups, exhibited minimal changes to the lipid bilayer (51).

The mass density profiles, hydrogen bond analysis, and distance measurements collectively elucidate the localization preferences of the alkaloids within the lipid bilayer. Mitragynine and mitragynine pseudoindoxyl predominantly localized near the lipid-water interface, as evidenced by their closer proximity to the lipid headgroups (average distances of 1.23 ± 0.71 nm and 2.40 ± 0.31 nm, respectively) and consistent

hydrogen bonding with both water and lipid headgroups. This positioning reflects their balanced affinity for both hydrophilic and hydrophobic environments, allowing them to maintain interactions with the aqueous phase while embedding into the lipid bilayer. The ability of these alkaloids to form multiple hydrogen bonds with lipid headgroups likely contributes to their stable positioning within the bilayer, potentially influencing membrane properties such as fluidity and permeability. Similar behavior has been observed in studies of other small molecules, such as flavonoids and anesthetics, which also form hydrogen bonds with lipid headgroups to stabilize their position in membranes (27, 52). In contrast, 7-hydroxymitragynine exhibited a stronger preference for the hydrophobic core, as indicated by its deeper penetration into the bilayer (average distance of 3.62 ± 0.27 nm from the lipid headgroups) and intermittent hydrogen bonding with lipid headgroups. This behavior aligns with its distance analysis and mass density profile, which shows the average positions of 7-hydroxymitragynine located deeper within the bilayer, farther from the polar headgroup region. The 7-hydroxymitragynine localization likely reduces its accessibility to the lipid headgroups, explaining the fewer and less stable hydrogen bonds observed. This is analogous to the behavior of cholesterol, which also resides deep within the hydrophobic core and forms minimal hydrogen bonds with lipid headgroups (53).

The results of this study provide valuable insights of kratom alkaloids interacting with the lipid bilayer. However, it is important to note that these findings are based on simulations representing only a single alkaloid molecule in the lipid bilayer system. In biological systems, higher concentrations of alkaloids or the presence of multiple alkaloid types within the cell membrane could lead to significantly different behaviors. For example, molecular aggregation—a phenomenon well-documented for other bioactive compounds—could profoundly alter membrane interactions. A report on fentanyl has demonstrated that molecular aggregation reduces membrane permeability and modifies pharmacological activity (54). Similarly, morphine molecules have been shown to form assemblies that interact strongly with lipid phosphate groups while embedding in the hydrophobic region (12, 17). These findings highlight the critical role of molecular aggregation in drug delivery systems, as it can markedly influence drug bioavailability and efficacy. This is further supported by studies on curcumin and doxorubicin, where aggregation has been shown to reduce membrane permeability due to the increased effective size of the drug molecules (55-57). The assembly of bioactive compounds in the aqueous phase before entering the lipid bilayer can prevent or delay the permeability, and potentially disrupt the cell membrane if the assembled molecules traverse the bilayer. These possibilities emphasized the need for further studies to explore the effects of alkaloid concentration, mixtures, and aggregation on membrane dynamics.

5.0 Conclusion

This is the first study that provides detailed insights into the membrane interactions of three kratom alkaloids – mitragynine, 7-hydroxymitragynine, and mitragynine pseudoindoxyl—using MD simulations. The results reveal that all three alkaloids rapidly permeate into the lipid bilayer, but their localization preferences slightly differ. Mitragynine and mitragynine pseudoindoxyl predominantly localized near the lipid-water interface, maintaining interactions with both water and lipid headgroups, while 7-hydroxymitragynine exhibits a stronger preference for the hydrophobic core, as evidenced by its deeper penetration and

reduced hydrogen bonding with lipid headgroups. These behaviors are supported by mass density profiles, hydrogen bond analysis, and distance measurements, which collectively highlight the influence of the physicochemical and amphiphilic properties of the alkaloids on their membrane interactions. Nevertheless, the study is limited to single-molecule systems, and future work should explore the effects of higher concentrations, alkaloid mixtures, and potential molecular aggregation on membrane dynamics. Such investigations will further elucidate the pharmacological implications of kratom alkaloids and their potential as therapeutic agents.

Author Contributions

NSMZ: Carried out the experiments, performed analysis and drafted the manuscript; **NSMZ, NAAA, NAA, SAJ, SWIS:** Manuscript review and editing; **SAJ:** Conceptualization and supervision; **AA and SAJ**: Project administration. All authors have read and agreed to the published version of the manuscript.

Acknowledgements

This research project was supported by the *Geran Inisiatif Penyeliaan* (GIP) 600-RMC/GIP 5/3 (080/2023)-Universiti Teknologi MARA (UiTM), Malaysia.

Conflict of Interest

All authors declare that there is no conflict of interests regarding the publication of this manuscript.

References

1. Malaysia Poisons Act 1952 and Regulation (Act 366). Kuala Lumpur: International Law Book Services (ILBS); 1952.

2. Charoenratana S, Anukul C, Aramrattana A. Attitudes towards Kratom use, decriminalization and the development of a community-based Kratom control mechanism in Southern Thailand. Int J Drug Policy. 2021; 95:103197.

3. Brown PN, Lund JA, Murch SJ. A botanical, phytochemical and ethnomedicinal review of the genus *Mitragyna korth*: Implications for products sold as kratom. J Ethnopharmacol. 2017; 18; 202:302–25.

4. Hill K, Rogers JM, Grundmann O, Epstein DH, Smith KE. At least four groups of kratom consumers in the United States: Latent-class analysis of motivations for kratom use. Am J Drug Alcohol Abuse. 2025; 51(2):191–203.

5. Swogger MT, Hart E, Erowid F, Erowid E, Trabold N, Yee K, *et al*. Experiences of kratom users: A qualitative analysis. J Psychoactive Drugs. 2015; 47(5):360–7.

6. Ahmad K, Aziz Z. *Mitragyna speciosa* use in the northern states of Malaysia: A cross-sectional study. J Ethnopharmacol. 2012; 141:446–50.

7. Anand A, Hosanagar A. The addictive potential and challenges with use of the 'herbal supplement' kratom: A case report and literature review. Pain Med. 2022;23(1):4–9.

8. Chamblee REA. A study of the kratom alkaloids and their binding to the μ-opioid receptor [Undergraduate thesis]. University of Mississippi; 2019 [cited 2024 Nov 5]. Available from: https://egrove.olemiss.edu/hon_thesis/1147

9. Todd DA, Kellogg JJ, Wallace ED, Khin M, Flores-Bocanegra L, Tanna RS, *et al*. Chemical composition and biological effects of kratom (*Mitragyna speciosa*): In vitro studies with implications for efficacy and drug interactions. Sci Rep. 2020;10(1):19158.

10. Flores-Bocanegra L, Raja HA, Graf TN, Augustinović M, Wallace ED, Hematian S, *et al*. The chemistry of kratom (*Mitragyna speciosa*): Updated characterization data and methods to elucidate indole and oxindole alkaloids. J Nat Prod. 2020;83(7):2165–77.

11. Ellis CR, Racz R, Kruhlak NL, Kim MT, Zakharov AV, Southall N, *et al*. Evaluating kratom alkaloids using PHASE. PLoS One. 2020;15(3):e0229646.

12. Kruegel AC, Grundmann O. The medicinal chemistry and neuropharmacology of kratom: A preliminary discussion of a promising medicinal plant and analysis of its potential for abuse. Neuropharmacol. 2018; 134:108–20.

13. Kruegel AC, Uprety R, Grinnell SG, Langreck C, Pekarskaya EA, Le Rouzic V, *et al.* 7-Hydroxymitragynine is an active metabolite of mitragynine and a key mediator of its analgesic effects. ACS Cent Sci. 2019;5(6):992–1001.

14. Angladon MA, Fossépré M, Leherte L, Vercauteren DP. Interaction of POPC, DPPC, and POPE with the μ-opioid receptor: A coarse-grained molecular dynamics study. PLoS One. 2019;14(3):e0213646.

15. Murray A, Hagen NA. Hydromorphone. J Pain Symptom Manage. 2005;29(5):57–66.

16. Trang T, Al-Hasani R, Salvemini D, Salter MW, Gutstein H, Cahill CM. Pain and poppies: The good, the bad, and the ugly of opioid analgesics. J Neurosci. 2015;35(41):13879–88.

17. Váradi A, Marrone GF, Palmer TC, Narayan A, Szabó MR, Le Rouzic V, *et al*. Mitragynine/corynantheidine pseudoindoxyls as opioid analgesics with mu agonism and delta antagonism, which do not recruit β-arrestin-2. J Med Chem. 2016;59(18):8381–97.

18. Hassan Z, Muzaimi M, Navaratnam V, Yusoff NHM, Suhaimi FW, Vadivelu R, *et al*. From Kratom to mitragynine and its derivatives: Physiological and behavioural effects related to use, abuse, and addiction. Neurosci Biobehav Rev. 2013; 37(2):138–51.

19. Matsumoto K, Horie S, Ishikawa H, Takayama H, Aimi N, Ponglux D, *et al*. Antinociceptive effect of 7-hydroxymitragynine in mice: Discovery of an orally active opioid analgesic from the Thai medicinal herb Mitragyna speciosa. Life Sci. 2004; 74(17):2143–55.

20 Yamamoto LT, Horie S, Takayama H, Aimi N, Sakai S-ichiro, Yano S, *et al*. Opioid receptor agonistic characteristics of mitragynine pseudoindoxyl in comparison with mitragynine derived from Thai medicinal plant *Mitragyna speciosa*. Gen Pharmacol. 1999; 33(1):73–81.

21. Ramos-Matos CF, Bistas KG, Lopez-Ojeda W. Fentanyl. In: StatPearls. Treasure Island (FL): StatPearls Publishing; 2023 May 29 [cited 2024 Oct 7]. Available from: http://www.ncbi.nlm.nih.gov/books/NBK459275/

22. Tsai MHM, Chen L, Baumann MH, Canals M, Javitch JA, Lane JR, *et al*. The in vitro functional profiles of fentanyl and nitazene analogs at the μ-opioid receptor—high efficacy is dangerous regardless of signaling bias. bioRxiv. 2023; 2023.11.10.566672.

23. Sutcliffe KJ, Corey RA, Alhosan N, Cavallo D, Groom S, Santiago M, *et al*. Interaction with the lipid membrane influences fentanyl pharmacology. Adv Drug Alcohol Res. 2022; 2:10280.

24. Vo QN, Mahinthichaichan P, Shen J, Ellis CR. How the μ-opioid receptor recognizes fentanyl. Nat Commun. 2021; 12(1):984.

25. Takayama H, Ishikawa H, Kurihara M, Kitajima M, Aimi N, Ponglux D, *et al*. Studies on the synthesis and opioid agonistic activities of Mitragynine-related indole alkaloids: Discovery of opioid agonists structurally different from other opioid ligands. J Med Chem. 2002; 45(9):1949–56.

26. Hossain SI, Saha SC, Deplazes E. Phenolic compounds alter the ion permeability of phospholipid bilayers via specific lipid interactions. Phys Chem Chem Phys. 2021; 23(39):22352–66.

27. Kopeć W, Telenius J, Khandelia H. Molecular dynamics simulations of the interactions of medicinal plant extracts and drugs with lipid bilayer membranes. FEBS J. 2013; 280(12):2785–805.

28. Hurst DP, Grossfield A, Lynch DL, Feller S, Romo TD, Gawrisch K, et al. A lipid pathway for ligand binding is necessary for a cannabinoid G protein-coupled receptor. J Biol Chem. 2010; 285(23):17954–64.

29. Swift RV, Jusoh SA, Offutt TL, Li ES, Amaro RE. Knowledge-based methods to train and

optimize virtual screening ensembles. J Chem Inf Model. 2016; 56(5):830–42.

30. Sztain T, Amaro R, McCammon JA. Elucidation of cryptic and allosteric pockets within the SARS-CoV-2 main protease. J Chem Inf Model. 2021; 61(7):3495–501.

31. Tang H, Demir Ö, Kurniawan F, Brown WL, Shi K, Moeller NH, *et al*. Structural characterization of a minimal antibody against human APOBEC3B. Viruses. 2021; 13(4):663.

32. Dror RO, Green HF, Valant C, Borhani DW, Valcourt JR, Pan AC, *et al*. Structural basis for modulation of a G-protein-coupled receptor by allosteric drugs. Nature. 2013; 503(7475):295–9.

33. Bennett WFD, Tieleman DP. Computer simulations of lipid membrane domains. Biochim Biophys Acta. 2013; 1828(8):1765–76.

34. Malde AK, Zuo L, Breeze M, Stroet M, Poger D, Nair PC, *et al*. An automated force field topology builder (ATB) and repository: Version 1.0. J Chem Theory Comput. 2011; 7(12):4026–37.

35. Jusoh SA, Helms V. Helical integrity and microsolvation of transmembrane domains from Flaviviridae envelope glycoproteins. Biochim Biophys Acta. 2011; 1808(4):1040–9.

36. Abraham MJ, Murtola T, Schulz R, Páll S, Smith JC, Hess B, *et al*. GROMACS: High-performance molecular simulations through multi-level parallelism from laptops to supercomputers. SoftwareX. 2015; 1:19–25.

37. Berendsen HJC, van der Spoel D, van Drunen R. GROMACS: A message-passing parallel molecular dynamics implementation. Comput Phys Commun. 1995; 91(1):43–56.

38. Poger D, Van Gunsteren WF, Mark AE. A new force field for simulating phosphatidylcholine bilayers. J Comput Chem. 2010; 31(6):1117–25.

39. Tieleman DP, Berendsen HJC. Molecular dynamics simulations of a fully hydrated dipalmitoylphosphatidylcholine bilayer with different macroscopic boundary conditions and parameters. J Chem Phys. 1996; 105(11):4871–80.

40. Darden T, York D, Pedersen L. Particle mesh Ewald: An N-log(N) method for Ewald sums in large systems. J Chem Phys. 1993; 98(12):10089–92.

41. Hess B, Bekker H, Berendsen HJC, Fraaije JGEM. LINCS: A linear constraint solver for molecular simulations. J Comput Chem. 1997; 18(12):1463–72.

42. Racine J. Gnuplot 4.0: A portable interactive plotting utility. J Appl Econom. 2006; 21(1):133–41.

43 Schrödinger, LLC. The PyMOL Molecular Graphics System, Version 1.8. New York, NY, USA: Schrödinger, LLC; 2015.

44. Yuan S, Chan HCS, Hu Z. Using PyMOL as a platform for computational drug design. WIREs Comput Mol Sci. 2017; 7(2):e1298.

45. Allen WJ, Lemkul JA, Bevan DR. GridMAT-MD: A grid-based membrane analysis tool for use with molecular dynamics. J Comput Chem. 2009; 30(12):1952–8.

46. Prates Ramalho JP, Gkeka P, Sarkisov L. Structure and phase transformations of DPPC lipid bilayers in the presence of nanoparticles: Insights from coarse-grained molecular dynamics simulations. Langmuir. 2011; 27(7):3723–30.

47. Ganjali Koli M, Azizi K. The partition and transport behavior of cytotoxic ionic liquids (ILs) through the DPPC bilayer: Insights from molecular dynamics simulation. Mol Membr Biol. 2016; 33(3–5):64–75.

48. Wang S, Larson R. Water channel formation and ion transport in linear and branched lipid bilayers. Phys Chem Chem Phys. 2014; 16(34):18338–45.

49. Nagle JF, Tristram-Nagle S. Structure of lipid bilayers. Biochim Biophys Acta. 2000; 1469(3):159–95.

50. Patra M, Karttunen M, Hyvönen MT, Falck E, Vattulainen I. Lipid bilayers driven to a wrong lane in molecular dynamics simulations by subtle changes in long-range electrostatic interactions. J Phys Chem B. 2004;

108(14):4485–94.

51. Faulkner KT, Robertson MP, Wilson JRU. Stronger regional biosecurity is essential to prevent hundreds of harmful biological invasions. Global Change Biol. 2020; 26(4):2449–62.

52. Lee J, Cheng X, Swails JM, Yeom MS, Eastman PK, Lemkul JA, *et al*. CHARMM-GUI input generator for NAMD, GROMACS, AMBER, OpenMM, and CHARMM/OpenMM simulations using the CHARMM36 additive force field. J Chem Theory Comput. 2016; 12(1):405–13.

53. Mouritsen OG, Zuckermann MJ. What's so special about cholesterol? Lipids. 2004; 39(11):1101–13.

54. Vuckovic D, Shirey R, Chen Y, Sidisky L, Aurand C, Stenerson K, *et al*. In vitro evaluation of new biocompatible coatings for solid-phase microextraction: Implications for drug analysis and in vivo sampling applications. Anal Chim Acta. 2009; 638(2):175–85.

55. Kunwar A, Barik A, Pandey R, Priyadarsini KI. Transport of liposomal and albumin loaded curcumin to living cells: An absorption and fluorescence spectroscopic study. Biochim Biophys Acta. 2006; 1760(10):1513–20.

56. Tacar O, Sriamornsak P, Dass CR. Doxorubicin: An update on anticancer molecular action, toxicity and novel drug delivery systems. J Pharm Pharmacol. 2012; 65(2):157–70.

57. Wang S. Transdermal delivery of cyclosporin-A using electroporation. J Control Release. 1998; 50(1–3):61–70.